ACS APPLIED MATERIALS & INTERFACES

Research Article

www.acsami.org

Electrochemical Performance and Durability of Carbon Supported Pt Catalyst in Contact with Aqueous and Polymeric Proton Conductors

Shuang Ma Andersen* and Eivind Skou

Department of Chemical Engineering, Biotechnology and Environmental Technology, University of Southern Denmark, Niels Bohrs Allé 1, DK-5230, Odense M, Denmark

Supporting Information

ABSTRACT: Significant differences in catalyst performance and durability are often observed between the use of a liquid electrolyte (e.g., sulfuric acid), and a solid polymer electrolyte (e.g., Nafion). To understand this phenomenon, we studied the electrochemical behavior of a commercially available carbon supported platinum catalyst in four different electrode structures: catalyst powder (CP), catalyst ionomer electrode (CIE), half membrane electrode assembly (HMEA), and full membrane electrode assembly (FMEA) in both ex situ and in situ experiments under a simulated start/stop cycle. We found that the catalyst performance and stability are very much influenced by the presence of the Nafion ionomers. The proton conducting phase provided by the ionomer and the self-assembled electrode structure render the catalysts a higher utilization and better stability. This is probably due to an enhanced dispersion, an improved proton−catalyst interface, the restriction of catalyst particle aggregation, and the improved stability of the ionomer phase especially after the lamination. Therefore, an innovative electrode HMEA design for ex-situ catalyst characterization is proposed. The electrode structure is identical to the one used in a real fuel cell, where the protons transport takes place solely through solid state proton conducting phase.

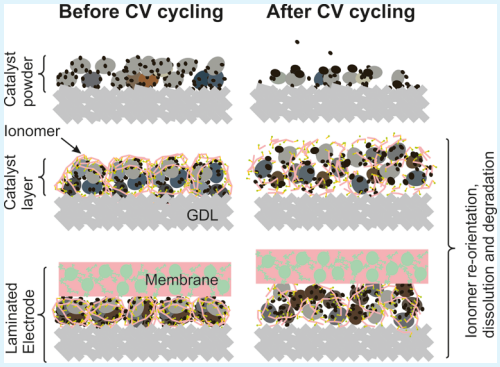

KEYWORDS: *interface, durability, PEMFC, MEA, Pt catalyst, electrode structure*

1. INTRODUCTION

Proton exchange membrane fuel cells (PEMFCs) are gaining much attention from both the technological and political worlds, because of their fundamental working concept, rapid development momentum, and a huge application potential in both mobile and stationary energy supplying systems.[1] Enhanced performance, cheaper materials, and especially, better durability, are essential for the widespread application of the PEMFCs.

Within fundamental material research, the degradation of Pt-based PEMFC catalysts is generally categorized into two aspects:[2] corrosion of carbon support and degradation of catalytic metals. Furthermore, the two aspects interact with and exacerbate each other. Mitigation strategies to alleviate the degradations include developments of novel durable catalyst supports such as CNT,[3] CNF,[4−6] SiC,[7,8] and WC or WO_x;[9] coverage of precious metal with a thin layer of metal oxide such as silica;[10] or the more interesting approach of enhancing attachment between catalyst and support by functionalization with organic compounds.[11−13]

The increased carbon corrosion resistance and higher stability of these catalysts were reported by Xu et al.[11] for p-benzensulfonic acid functionalized Vulcan and high-surface-area carbon. Similarly, He et al.[12] demonstrated that Pt supported by perfluorosulfonic acid (PFSA) functionalized CNT showed 100% increase in durability in comparison with plain Pt/CNT. A similar result was reported by Cheng et al.[13] by using carbon black. Moreover, Nafion-stabilized colloid was also found to enhance catalyst lifetime.[14] The improved catalyst durability was due to a stronger attachment between the catalyst and the carbon, which prevents aggregation of the catalyst particles, as well as detachment from the supports. Here, interactions between organic compounds, catalysts and support materials demonstrate their noteworthy influence on the electrochemical performance of the catalysts.

The exploration of catalyst candidates for PEMFCs has been going on for more than two decades. However, a gap between the fundamental materials research and the final product application in a fuel cell is often experienced. Confined Nafion thin film is indispensable in an electrode structure to provide proton conduction; at the same time, it still allows electron conduction through tunneling.[15] The details of Nafion thin film is still not well understood, though fibrillar structure corresponding to elongated polymeric aggregates surrounded with the ionic charges is generally agreed in the literature.[16] The confined Nafion thin film plays a vital link between the pure catalyst research and fuel cell electrode performance study.

Received: May 12, 2014
Accepted: September 12, 2014
Published: September 12, 2014

dx.doi.org/10.1021/am5028956 | ACS Appl. Mater. Interfaces 2014, 6, 16565−16576

Most ex situ materials research is carried out with either free or with an extremely thin layer of Nafion film on top, which is a structure far away from the actual configuration of a membrane electrode assembly (MEA) as used in fuel cells. The discrepancies between fuel cell catalyst performance and an ordinary ex situ catalyst study lies in the following aspects:

1). Ionomer Content and Component Mixing. The optimized ionomer content of a PEMFC catalyst layer is usually between 20 and 50 wt %.[17−19] Hardly any catalyst research is carried out with such high ionomer loading. Even a thin layer of ionomer is applied on the top of catalysts, there is minimal contact between the ionomers and the catalyst particles, in contrast to the interactions in a three-dimensional fuel cell electrode. Moreover, there is hardly any interaction between the ionomers and the catalysts because they are not mixed freely in an aqueous phase, which is how a catalyst paste is prepared for screen or spray printing.[20]

2). Proton Conducting Phase. During an ordinary ex situ experiment, the catalysts are usually immerged in a liquid electrolyte. Even when an ionomer phase is correctly prepared in the electrode, ionomer degradation is hard to be monitored by following the change of Pt active surface area, because the additional liquid electrolyte can continue to provide protons, which is not the case in a fuel cell. Moreover, Nafion thin film is reported to have different morphologies depending on it is in contact with liquid water or water vapor.[21] Finally, catalyst characterization in aqueous environment is often sensitive toward ion interference.[22]

3). Electrode Structure. A lamination procedure including hot pressing is often used during MEA production. Generally, high temperature and high pressure is applied in order to produce the ultimate electrode structure. The electrode morphology and performance of the catalyst layer show significant differences before and after the hot pressing,[23] or under different lamination conditions as suggested by others.[24] Pressure was found to be one of the critical parameters. Jia et al.,[25] demonstrated that even cold pressing can lead to improved cell performance.

Therefore, knowledge from ordinary ex situ materials research can often not be directly transferred to the development of a fuel cell system.

He et al.,[26] studied graphite supported Pt nanoparticle adhesion/aggregation in an environment of a 1 nm thick Nafion coating based on classic molecular dynamics simulations. They pointed out that adhesion forces will decrease (less particle aggregation) as the hydration level goes up. Furthermore, the extent of the decrease will be affected by the interaction between the graphite surface and Nafion. The choice of graphite is because of its well-defined atomic lattice being a convenient parameter for the simulation. In this sense, highly amorphous carbon black might bring a challenge for such work. However, the knowledge of catalyst aggregation under the influence of a proton conducting polymer (as an indispensable component of the electrode) could be extremely valuable for both researchers and industries in the energy sector.

Despite a large tendency for carbon corrosion and fast catalyst degradation, high-surface-area carbon black is still one of the most favored ingredients of the electrode, and demonstrates state of the art performance as validated by fuel cell and MEA producers. The gap between basic material property studies and fuel cell system application is likely due to the intricate component interactions: addition of the Nafion ionomer in catalyst layer alleviates carbon corrosion and diminishes catalyst aggregation/detachment. As a result, carbon corrosion and reduction of platinum surface area may not be the bottleneck of a fuel cell performance anymore. On the other hand, robustness of the proton conducting ionomer may be the crucial parameter to maintain platinum accessibility.

In our earlier work, we documented that there are intense interactions (of different degree) between Nafion ionomers and various catalysts and catalyst supports[27−29] and there is an optimum content of the ionomer in an electrode.[17] In the present work, we focus on the electrochemical performance and durability of the catalyst in relation to ionomer and membrane electrode assembly environment to demonstrate that catalyst performance is component and process dependent. A more reasonable approach of catalyst evaluation should take both electrode components and electrode structure into account, since both contribute to the final delicate morphology of the three-phase boundary (TPB) in an electrode. Moreover, a simulated start/stop potential cycling treatment was applied on the samples. Such events in real life, when not well managed, are known to be the most harmful regarding the stability of the PEMFC components,[30] because formation of an air/fuel boundary at the anode will significantly increase the local electrode potential at the cathode to a value as high as 1.6 V.[31]

2. EXPERIMENTAL SECTION

2.1. Sample Preparation and Nomenclature. 57 wt % Pt supported on high-surface-area carbon black, Hispec 9100 (Johnson Matthey) was used as received. Transmission electron microscopy (TEM) (see the Supporting Information, Figure S1) reveals that there is a reasonable dispersion of the platinum particles over the carbon support. The catalyst diameter shows the highest population within 2−3 nm. This corresponds well with the information provided by the catalyst supplier[32] and in house X-ray diffraction measurement.

A catalyst powder (CP) sample was prepared by drop coating of well ultrasonicated catalyst powder in water suspension on a piece of carbon paper (Toray Industries). The final weight was determined by weighing before and after applying the coating. A catalyst ionomer electrode (CIE) sample was prepared following a standard PEMFC electrode preparation recipe,[6,20] where a catalyst−water/alcohol suspension of 30% Nafion ionomer (w/w) was coated onto a gas diffusion layer (GDL) Sigracet 35DC (SGL Group). A half membrane electrode assembly (HMEA) sample was constructed by laminating the electrode coated GDL onto membrane Nafion 212 at 140 °C and 7 bar for 3 min. A full membrane electrode assembly (FMEA) sample was assembled in the same way as HMEA, except that Nafion was sandwiched between two electrode coated GDLs instead. FMEA is expected of the same electrode structure as HMEA, since the same fabrication condition was applied. FMEA-A denotes the anode of the FMEA. A catalyst loading of 0.5 mg Pt/cm^2 was applied for all electrodes. CIE, HMEA and FMEA of the optimized structure were provided by IRD Fuel Cells A/S.

2.2. HMEA Electrochemical Measurements. An innovative electrode design−HMEA is proposed for ex-situ experiments. The catalyst layer is indirectly connected with the aqueous electrolyte through Nafion membrane. A rubber sealing around the edge was used to prevent any liquid in contact with the catalyst layer. So the catalysts exposing themselves toward the gas phase receive solely protons through the ionomer. A sketch of the cell design is available in the Supporting Information, Figure S2.

CP, CIE, and HMEA samples were used as working electrode (WE) to perform cyclic voltammetry (CV) in a conventional three electrodes wet cell. A radiometer $Hg/HgSO_4$ electrode was used as the reference electrode (RE). All potential values are reported versus (vs) reversible hydrogen electrode (RHE). A glassy carbon rod was used as the counter electrode (CE). The liquid electrolyte was 1 M H_2SO_4 (Sigma-Aldrich). The CV treatment was applied between 0.4 and

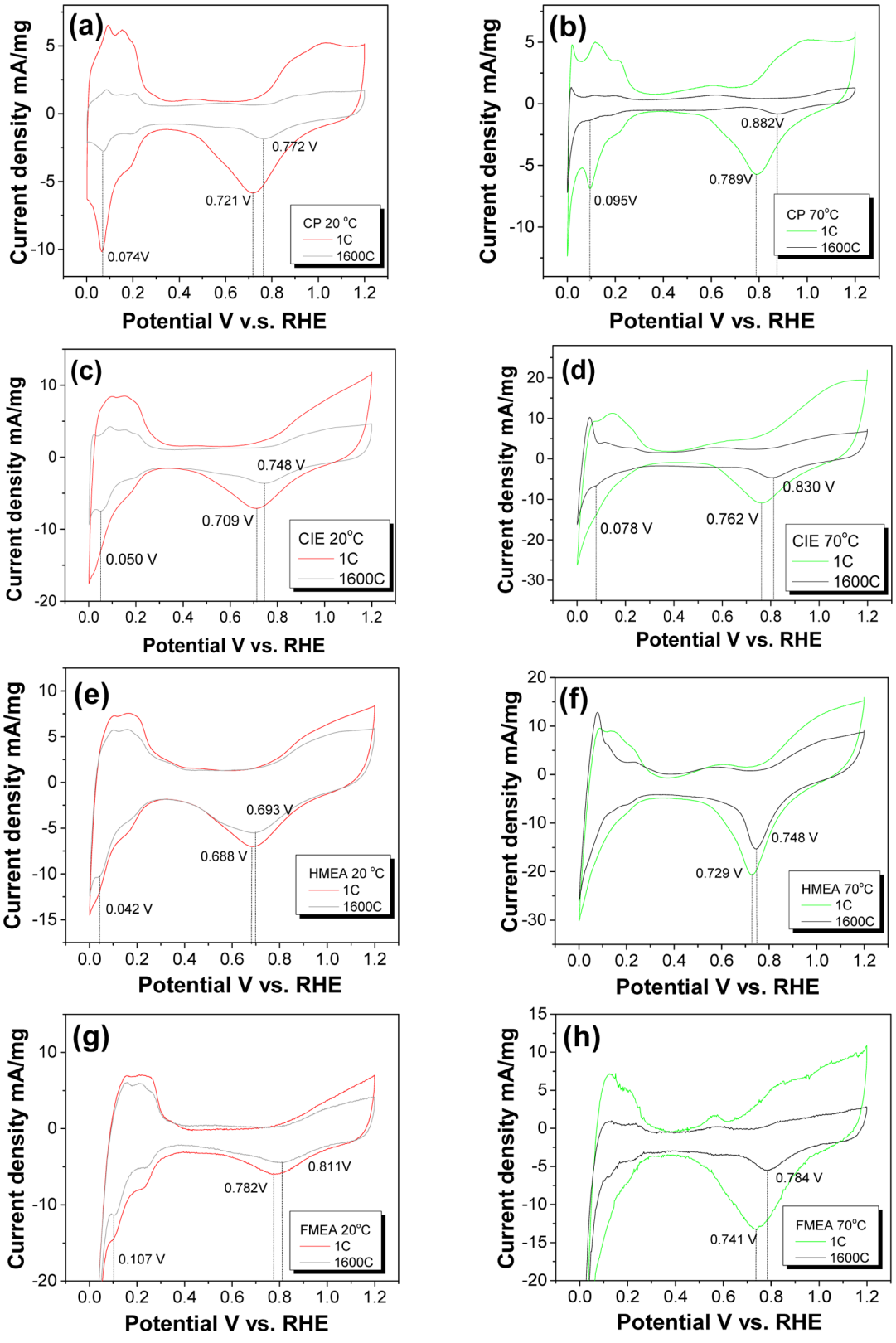

Figure 1. CV performance of CP, CIE, HMEA, and FMEA at 20 and 70 °C. Platinum oxide reduction and hydrogen adsorption peaks are labeled in the figure (due to the dominating hydrogen evolution, hydrogen adsorption is not detectable in panels f and h).

1.6 V with a scan rate of 1 V/s. The CV evaluation was performed between 0 and 1.2 V, with a scan rate of 10 mV/s. The first cycle is abandoned (due to wetting, impurity, system stabilization etc.), the second cycle is reported in this work (labeled as cycle 1). Ar purging was maintained during the measurements with a constant flow of 0.2 mL/s. The experiments were carried out with an electrochemical workstation (Zahner IM6e). The connection between the sample and the device was established with a 0.2 mm thick gold wire.

The evaluation of platinum surface area was carried out by determining columbic charge transfer of monolayer atomic hydrogen

dx.doi.org/10.1021/am5028956 | ACS Appl. Mater. Interfaces 2014, 6, 16565−16576

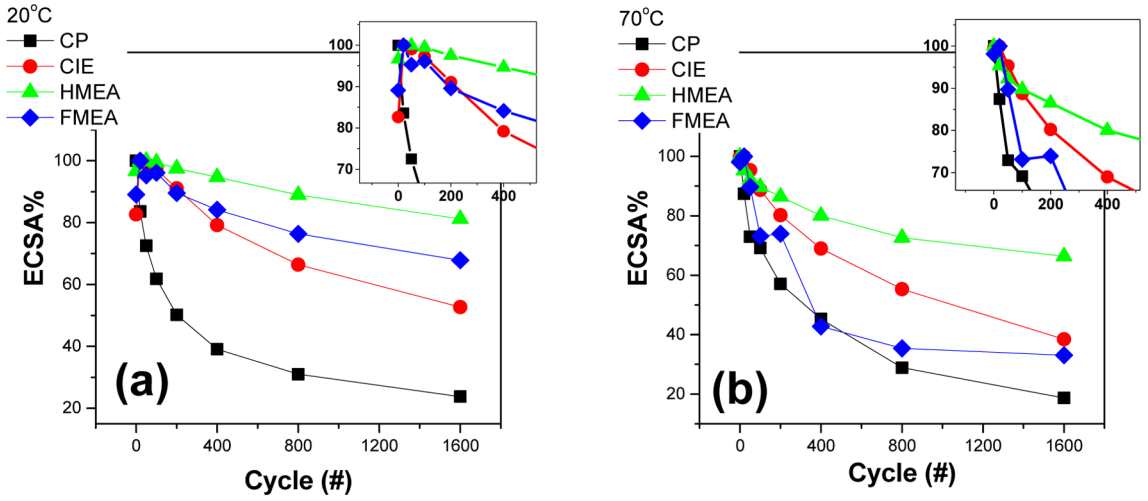

Figure 2. ECSA change of different electrodes at 20 and 70 °C.

adsorption. The electrochemical surface area (ECSA) was calculated with the following equation

$$\mathrm{ECSA} = \frac{Q}{[\mathrm{Pt}]AC}$$

Where ECSA is electrochemical surface area or platinum (m^2/g), Q is the charge for hydrogen adsorption, (C), [Pt] is platinum loading, (g/m^2), A is area, (m^2), and C is a constant, which is the charge required to oxidize a monolayer of atomic hydrogen on Pt catalyst, in the calculation $C = 2.2\ C/m^2$.[33]

The utilization of the catalyst was calculated as the corrected electrochemically active surface area (CECSA, section 4.4) of the platinum relative to its geometric surface area

$$U = \frac{\mathrm{CESCA}\left(\frac{4}{3}\pi \times r^3 d\right)}{4\pi r^2}100 = \frac{1}{3}\mathrm{CESCA}rd100$$

Where U is utilization (%), CECSA is corrected electrochemical surface area of platinum (m^2/g) (see section 4.4), r is average radius of the platinum catalyst (m), and d is density of platinum, 2.145×10^7 (g/m^3).

2.3. Other Characterization Methods. The powder X-ray diffraction (XRD) pattern was collected by using Panalytical X'Pert diffractometer. Data treatment was assisted by X'Pert HighScope Plus. CP and CIE samples were used directly for the measurement. For HMEA and FMEA samples, GDL was physically removed by peeling off the layer. Any residual carbon paper, which was identified by the fiber nature and gray color, was carefully removed with a sharp scalpel.

Dissolved platinum in the aqueous electrolyte was analyzed with a SHIMADZU atomic adsorption spectrotrometer (AAS) A-7000 equipped with a high sensitivity graphite furnace. The scanning electron microscope (SEM) was a Hitachi S-4800 system with a cold field-emission electron source for ultrahigh resolution and an energy-dispersive X-ray spectrometer (EDXS). Fuel cell testing was performed with a single cell of dimension $2.5 \times 2.5\ cm^2$. A fast cell activation step was carried out at 0.7 V with 7% hydrogen in argon as fuel and lab air as oxidant of flow 2.8 and 1 mL/s respectively, 100% humidity for 30 min. During potential cycling treatment and CV evaluation, 7% hydrogen in argon was purged on the anode, which serves as both counter and reference electrode, and pure argon was purged on the cathode, which was used as working electrode. The system was controlled and monitored by an electrochemical workstation (IM6, ZAHNER). All data are presented with Origin Pro 9.1.

3. RESULTS

3.1. Electrochemical Measurements. Potential cycling was performed, ex situ, in a three-electrode electrochemical cell on CP, CIE, and HMEA samples, and in situ, in a two-electrode single cell on FMEA samples. Cyclic voltammograms of first and last cycles are presented in Figure 1. CVs in hydrogen region at cycle 1, 20, 50, 100, 200, 400, 800, and 1600 are available in the Supporting Information, Figure S3.

3.1.1. Peak Position Shift. Both the hydrogen adsorption peak and the hydrogen desorption peak were found to shift slightly toward lower potential for ionomer containing samples (CIE and HMEA) compared to catalyst powder samples in all ex situ experiments (the lowest potential value of the hydrogen adsorption is indicated in Figure 1a–e and g). This is due to the fact that platinum and carbon support is covered with the ionomer (because of their strong affinity[27−29]), which might affect the hydrogen adsorption. Therefore, a smaller overpotential is required for adsorption and desorption. Moreover, for the catalyst powder samples under the slow sweep rate, distinct peaks of strongly (0.28 V vs RHE) and weakly (0.12 V vs RHE) bonded hydrogen[34,35] assigned to Pt (100) and the combination of Pt (110) and Pt (111) crystal faces, were observed. Even a third peak between these two peaks due to the oxidation of the subsurface hydrogen,[36] was also observed. However, the hydrogen region appeared blurred and unresolved for ionomer containing samples. This is also caused by the interaction among the components. Depending on the porosity of the support, the location of the catalyst and coverage by the ionomer, the overpotential might shift slightly and the current appears flattened out. CVs recorded under in situ single cell condition (FMEA) are found to shift to higher potentials. This is possibly due to a slightly mixed potential resulting from gas crossover, or the increased possibility to generate pH changes. All voltammograms shift to slightly higher potential at elevated temperatures.

A pair of broad peaks at between 0.4–0.7 V vs RHE were observed in Figure 1a, b, d, f, and h). They are likely to be the well-known hydroquinone–quinone (HQ–Q) redox couple on the carbon surface.[11] The appearance of the peaks in the voltammograms indicates carbon corrosion. This is especially evident for binder less catalyst powder after the CV treatment. Furthermore, the quinone redox couple was observed for all samples at elevated temperatures.

3.1.2. Evolution of the Electrochemical Surface Area (ECSA %). Changes in percentage of the electrochemical surface area (ECSA, referring to original platinum loading) are summarized in Figure 2. The highest ECSA obtained during the potential cycling was chosen as 100%. In general, for the ex-situ experiments, HMEA showed least degradation followed by CIE and CP. Elevated temperature was found to accelerate the reduction of ECSA in all the cases. At room temperature, ECSA of FMEA degraded 20% faster than HMEA. Large differences between HMEA and FMEA were observed at 70 °C, which will be discussed later.

3.1.3. Platinum Particle Size Change Reflected by the Peak Position Shift of Platinum Oxide Reduction. The relative position of the platinum oxide reduction peak is an indication of platinum particle size change.[37] Higher potential shift indicates larger degree of platinum particle aggregation. The values are marked individually in the cyclic voltammograms Figure 1 and summarized in Table 1.

Table 1. Platinum Oxide Reduction Peak Position[a]

	treatment					
	20 °C			70 °C		
sample	1c	1600c	Shift	1c	1600c	Shift
CP	0.721	0.772	0.051	0.789	0.882	0.093
CIE	0.709	0.748	0.039	0.762	0.83	0.068
HMEA	0.688	0.693	0.005	0.729	0.748	0.019
FMEA	0.782	0.811	0.029	0.741	0.784	0.043

[a]All values are in V vs. RHE.

The values indicate that the naked catalyst powder has the largest tendency for particle growth/coalescence among the three ex-situ samples, and then followed by CIE and HMEA samples. FMEA in the in situ experiment showed higher degree of Pt aggregation than HMEA. A similar trend was observed at 70 °C with a larger degree of aggregation for all the cases than at 20 °C.

3.2. X-ray Diffraction Characterization. Diffractograms of both ex-situ and in situ samples are shown in Figure 3.

In Figure 3a–e, the diffraction at around 2θ = 39.6, 45.9, 67.6, 81.70, and 86.8° can be assigned to the Pt (111), Pt (200), Pt (220), Pt (311), and Pt (222). Dominating peaks at approximate 2θ = 26.6, 54.7, 77.6, and 83.8° are due to the diffraction of highly graphitized carbon paper used as support electrode. In Figure 3b–e, a rather broad peak at approximate 2θ = 16–19° is due to the ionomer contribution in the electrode structure. Pt crystallite size was evaluated from peak broadening based on Scherrer formula from the Pt (111) peak, and the relative change is summarized in Table 2.

As shown in Figure 3f, Nafion has a diffraction peak at around 2θ = 39.7°, which incidentally overlaps with platinum (111) face. The content of the ionomer in the electrode structure shows influence on the peak widening. Consequently, platinum particle size calculated as using the Scherrer formula cannot be directly compared between catalyst powder and ionomer containing samples. Therefore, only relative changes are discussed. In general, the size of platinum crystallite increased with potential cycling and elevated temperatures.

In the case of ionomer containing samples (CIE, HMEA, and FMEA), the peak between 2θ = 16–19° is due to the ionomer contribution, as shown in Figure 4. Large differences were found between CIE and HMEA (or FMEA) samples. All CIE samples showed a sharp symmetric peak at 2θ = 18°, which corresponds to a crystalline diffraction similar to the perfluorocarbon backbone in Teflon. All laminated MEAs, showed an amorphous halo between 2θ = 16–19° with minor contribution from crystalline diffraction, which had great resemblance to Nafion membrane XRD pattern[38] as shown in Figure 4a. This indicates that the originally highly crystalline ionomer structure in CIE transforms into a less ordered structure in laminated HMEA and FMEA samples upon hot pressing. After the CV treatments, the crystallinity did not show detectable change in XRD.

3.3. Atomic Adsorption Spectroscopy. The dissolution of platinum in electrolyte solution was confirmed by AAS for all ex situ experiments and summarized in Figure 5. The values will be discussed in relation to other techniques in section 4.

No trace of platinum was found in exhaust water from the single cell after potential cycling operation. However, platinum particles (platinum band) were detected in the membrane electrolyte as shown in microscopy later.

3.4. SEM-EDXS Characterization. Cross sections of selective pristine and potential cycled (used) samples were examined with SEM-EDXS. Microscopic images can be found in the Supporting Information, Figure S4. A list of catalyst layer thickness and the relative changes after the treatment is summarized in Table 3.

The catalyst layer in pristine HMEA (or FMEA) was seen to be much thinner than the pristine CIE, which is due to the hot pressing step. In wet cell condition, catalyst layers of used CIE and HMEA were found to be thicker than their initial equivalents. This is probably due to free expansion of the ionomers in liquid media during treatment. In single cell used FMEA sample, both anode and cathode were found to be slightly thinner than their original values. This might be due to restriction/pressure from both the graphite plates, plus possible degradation of the components.

For potential cycled single-cell FMEA, a platinum band was observed in the membrane electrolyte as shown in Figure 6a, b. However, no such band was detected in HMEA electrode as shown in Figure 6c, d.

The formation of a platinum band in the membrane electrolyte after fuel cell operation is commonly recognized as due to the reduction of the Pt ions (formed at the cathode during oxidation and migrated through hydrophilic domain of the proton conducting phase) by the hydrogen permeated from the anode.[39,40] Therefore, the relative position of the platinum band in the membrane depends on both the platinum ion flux and the hydrogen permeability. In our case, 7% H_2 in argon was used as reducing agent for FMEA operation, which provides lower partial pressure of H_2. This causes the Pt band to be located relatively closer to the anode compared to others finding.[38] However, in the case of HMEA, no reducing agent was applied. Pt ions were found to migrate through the membrane and being detected in the liquid electrolyte. The majority of the Pt ions were found in the solution rather in the membrane, since the Pt ions are exchanged with protons from the electrolyte.

4. DISCUSSION

Although identical catalyst was applied in the four electrodes (CP, CIE, HMEA, FMEA), platinum exhibited very different degradation patterns. The reduction of the electrochemically active surface area of Pt is due to not only catalyst physical loss, platinum dissolution, platinum particle aggregation, and carbon

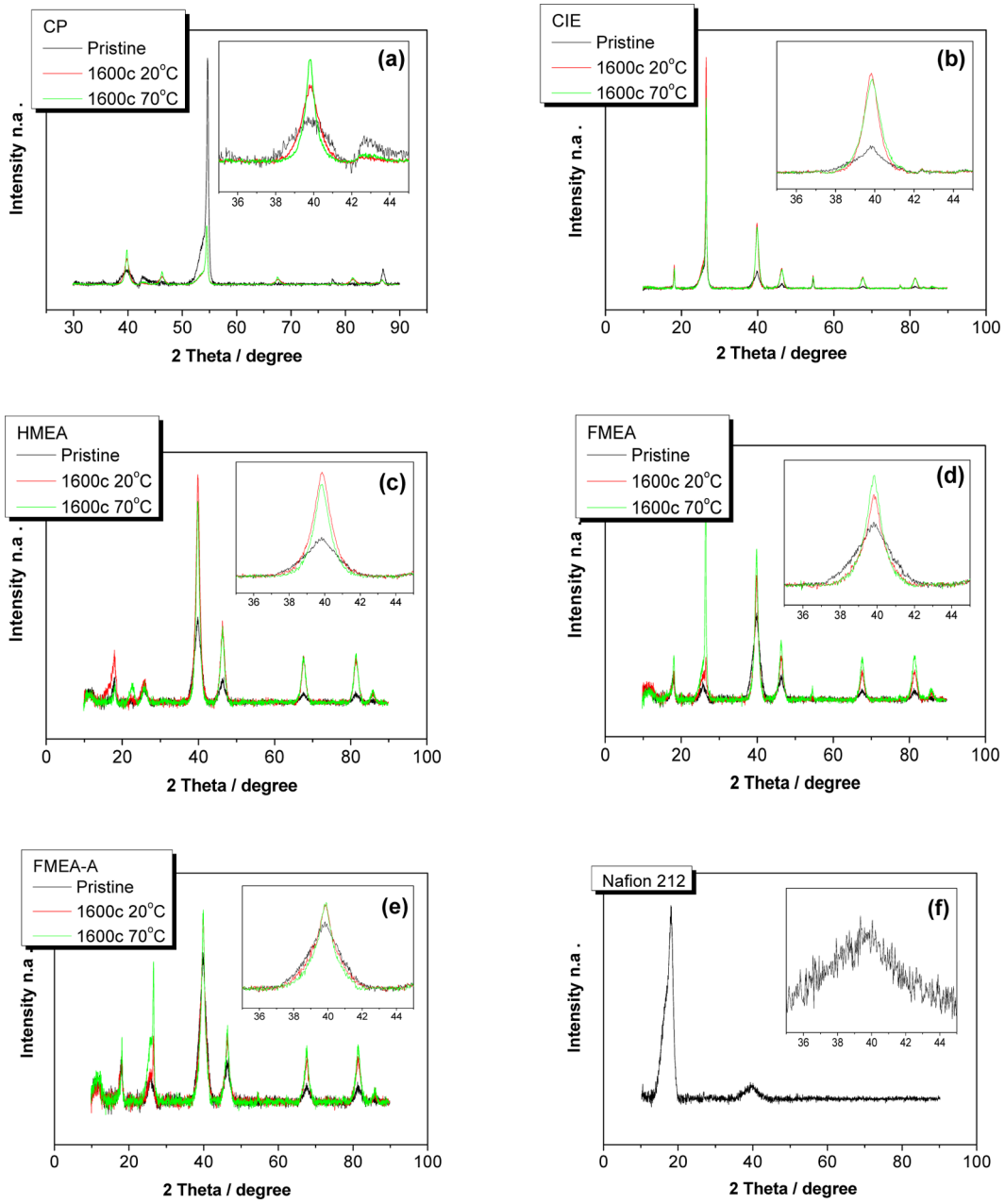

Figure 3. XRD of electrode samples with focus on platinum region.

Table 2. Relative Change of Platinum Crystal Size

sample	treatment	temp. (°C)	Pt size (%)
CP0	pristine	20	100
CP20	1600c	20	181
CP70	1600c	70	299
CIE0	pristine	20	100
CIE20	1600c	20	213
CIE70	1600c	70	203
HMEA0 & FMEA0	pristine	20	100
HMEA20	1600c	20	161
HMEA70	1600c	70	179
FMEA20	1600c	20	160
FMEA70	1600c	70	180
FMEA20-A	1600c	70	123
FMEA-70-A	1600c	70	149

corrosion but also to ionomer degradation and probably to property changes of pore morphology and surface. The latter was even more pronounced in the single cell configuration.

4.1. Initial ECSA. The initial ECSAs of the pristine samples are summarized in Table 4. ECSA is equal to CECSA (see 4.4) for the pristine samples. CP showed the lowest ECSA among the four electrodes. The relatively low value is due to the high porosity of the catalyst support. The catalysts trapped in microspores are not accessible to aqueous electrolyte. In the case of ionomer containing electrodes, the amphiphilic property of the polymer could assist the wetting of the interface. For CIE, some of the catalyst particles trapped in the pores could be in contact with the ionomer,[41] and thus showing improved utilization. For HMEA, slightly lower ECSA was observed. The difference is possibly due to two-phase active Pt and three-phase active Pt. For two phase-active Pt (electron and proton, since gas channels are replaced by the liquid electrolyte),

dx.doi.org/10.1021/am5028956 | ACS Appl. Mater. Interfaces 2014, 6, 16565−16576

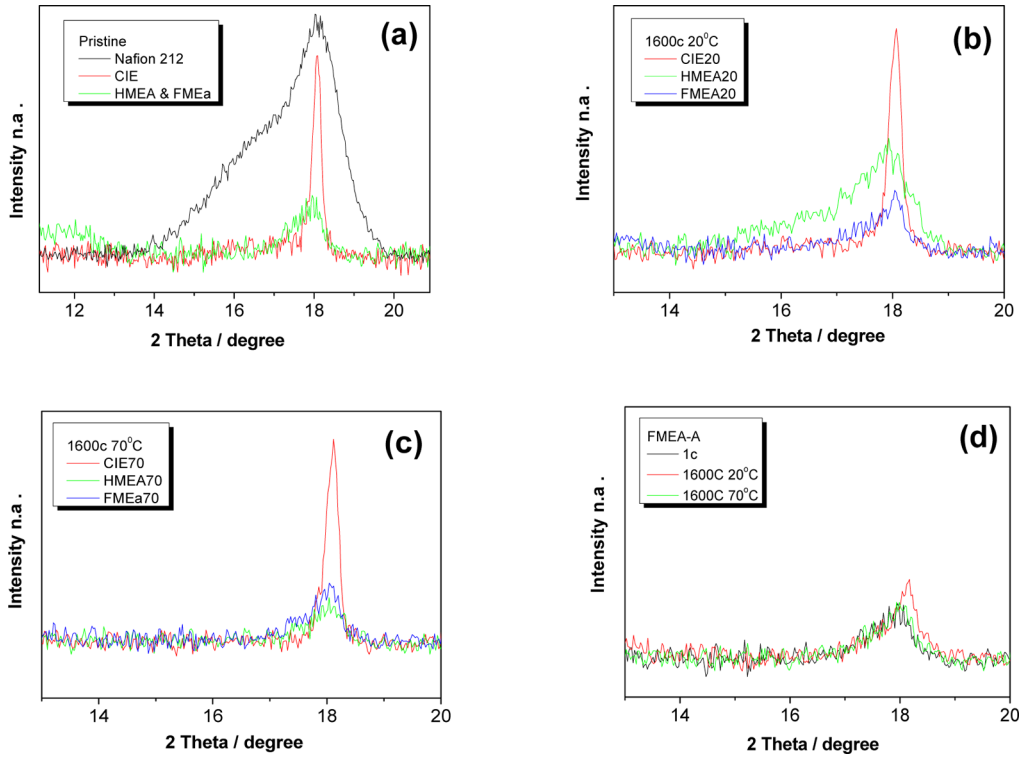

Figure 4. XRD of ionomer/polymer region for CIE, HMEA, FMEA, and FMEA-A samples.

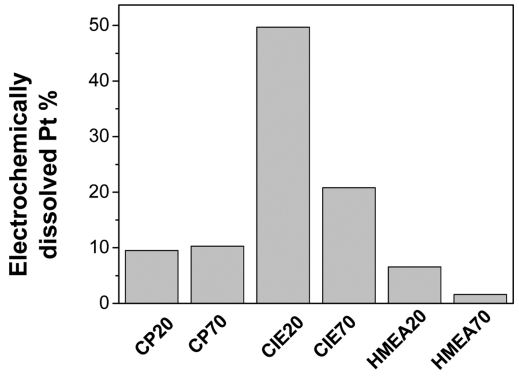

Figure 5. Platinum losses in % due to electrochemical dissolution.

Table 3. List of the Catalyst Layer Thickness

ID	history	thickness (μm)	thickness (%)
CIE	pristine	261	100
CIE	used	322	124
HMEA/FMEA	pristine	21	100
HMEA	used	61	290
FMEA	used	14	56
FMEA-A	used	13	84

protons can be transported through either ionomer or liquid electrolyte via gas channels, as the case for CIE, whereas in HMEA, the ionomer has the foremost influence to the proton phase, through either its intrinsic proton conductivity or influence of water distribution.[42] So, the ionomer with its associated water network conducts protons to the three-phase active Pt (electron, proton and gas). For FMEA, slightly higher ECSA than HMEA's was observed. The higher value is possibly due to the compact cell configuration and high pressure from both electrodes, which give rise to a better contact. ECSA was found to be slightly lower at high temperatures for ionomer containing samples. This is probably due to a lower degree of hydration of the polymer at elevated temperature. Because of the huge electrode component and preparation differences, a direct comparison of the ECSA from other groups is difficulty. For pure catalyst (Hispec 9100) study, ECSA (or CECSA) of the pristine state is comparable with others.[43−45]

4.2. Reorientation of the Ionomer during Potential Cycling. At room temperature, the catalyst powder samples showed a monotonic decrease of the electrochemical surface area with the increasing number of potential cycles. For ionomer containing samples there is a slight increase (up to 20% for CIE and around 5% for HMEA, as shown in Figure 2, 20 °C) of ECSA within the first few tens of cycles, followed by a decline of ECSA with the increasing number of cycles. The increase at the beginning can be due, in part, to a self-cleaning process eliminating surface impurities, but more importantly, also a reorganization of the electrode−electrolyte interface, as observed by others.[21,46,47] The catalyst layer in the CIE sample has a combination of hydrophilic particles of porous catalyst on carbon and amphiphilic Nafion ionomers. The hydrophilic sulfonic end group of the ionomer is preferentially adsorbed to the metal catalyst and the porous carbon; this may lead to the hydrophobic fluorocarbon backbone being exposed to the surface.[29] The consequent hydrophobic surface does not wet well with a water-based electrolyte. This contact problem may be alleviated during potential cycling, since the ionomer may reorient and oxidized carbon can enhance the wetting property of the interface. The improved wetting property of the catalyst-ionomer-electrode surface allows more catalyst to be accessible to the liquid electrolyte. Hence, ECSA increased in the first few tens of cycles. In addition, reorganized ionomers may get in touch with more catalyst trapped in the micropores of the high surface area carbon, which also contributes ECSA. MEAs (both

dx.doi.org/10.1021/am5028956 | ACS Appl. Mater. Interfaces 2014, 6, 16565−16576

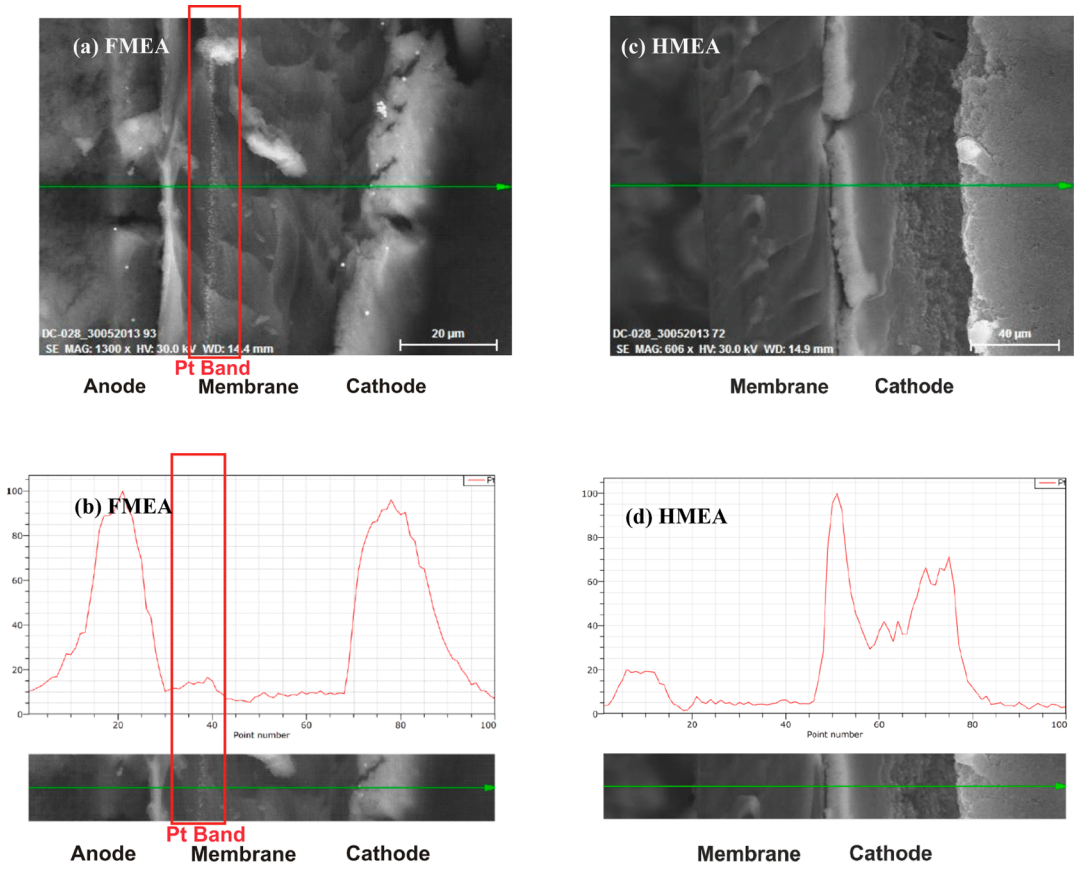

Figure 6. SEM-EDXS of FMEA and HMEA after potential cycling.

Table 4. CECSA and Utilization of the Pt Catalysts in Different Electrode Structures

ID	treatment	temp. (°C)	CECSA[#] (m^2/g)	CECSA (%)	utilization[§] (%)
CP0	pristine	20	52.8	100	79
CP20	1600c	20	14.5	27	37
CP0	pristine	70	54.5	100	82
CP70	1600c	70	12.9	24	54
CIE0	pristine	20	68.28[¤]	90	90
CIE20	1600c	20	62.1	98	186
CIE0	pristine	70	63.1	100	100
CIE70	1600c	70	26.5	42	69
HMEA0	pristine	20	58.8[¤]	97	75
HMEA20	1600c	20	52.4	91	113
HMEA0	pristine	70	57.4	100	77
HMEA70	1600c	70	33.4	58	80
FMEA0	pristine	20	64.9[¤]	98	80
FMEA20	1600c	20	51.0*	83*	95*
FMEA0	pristine	70	60.7	100	81
FMEA70	1600c	70	20.2*	33*	48*

[#]CECSA=ECSA for pristine samples, data deviation is within 2% based on repeated measurements. [¤]ECSA after the initial reorientation of the ionomer (see section 4.2). [*]Pt dissolution is estimated based on HMEA equivalent conditions. [§]Calculation of utilization is based on CECSA.

HMEA and FMEA) showed similar reorganization of the catalyst-ionomer structure during the initial potential cycling, but less extensively and require more cycles (first 100 cycles or slightly longer time). This may be due to the lower degree of freedom of the ionomer after the lamination procedure. At 70 °C, ionomer reorientation appeared much less obvious. This is probably because the higher temperature accelerates the process, which was completed at the beginning of the measurement.

4.3. Catalyst Physical Losses. For catalyst powder (CP) samples, potential cycling degradations at 20 and 70 °C display great resemblance: high ECSA losses (76 and 81%, Figure 2) and low Pt dissolution (9.5 and 10.3%, Figure 5). Besides, black particles were constantly observed on the bottom of the cell after the experiment for this type of sample. These indicate that particle falling (physical loss) due to gravity, vibration, turbulence and, especially, carbon corrosion is one of the major reasons for the surface area loss of platinum for binder less electrodes, as illustrated in Figure 7 (a). Depending on support-backing-materials (carbon paper in this case) or cell design (vertical in this case), there might be different affinity between the catalyst and the backing-material, which may lead to physical losses of different degrees, but of great importance.

4.4. Corrected Electrochemical Surface Area (CECSA). For a better comparison of various experiments, a new term is introduced: corrected electrochemical surface area (CECSA), which is similar to ECSA, but it corrects the original loading with the amount of platinum dissolved. It reflects the electrochemically active platinum surface area normalized to the actual platinum quantity in the system, which includes both active and inactive platinum catalyst. CECSA of the corresponding samples are summarized in Table 4.

Platinum dissolution also happened in FMEA, as illustrated by a platinum band detected in the membrane as shown in section 3.4. The dissolved amount was estimated based on HMEA Pt dissolution.

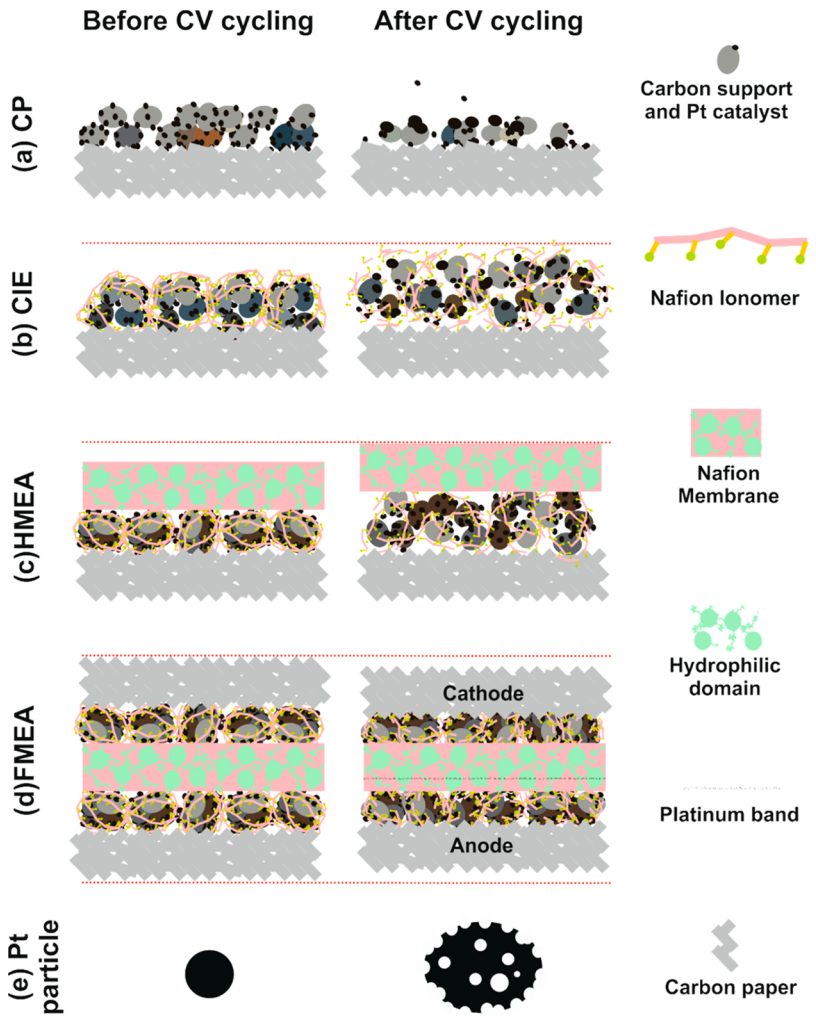

Figure 7. Electrode structure change before and after potential cycling (not to scale). The major effects are platinum aggregation, detachment or dissolution, carbon corrosion and ionomer degeneration; electrode expansion in liquid phase, slight reduction in gas phase.

4.5. Carbon Corrosion and Ionomer Degradation. At elevated temperatures, there was significantly greater loss of CECSA for ionomer containing samples. However, this was not due to a higher dissolution of platinum in aqueous electrolyte, as confirmed by AAS measurement (Section 3.3) and only partially due to platinum particle enlargement (Section 3.2). More likely, the decrease of the platinum electrochemical surface area was due to a combination of interphase degradation including carbon corrosion and ionomer degradation.

Carbon corrosion affects the electronic conductive phase. The corrosion reaction is well-known and is severe at high temperatures.[48] It was also reflected in the cyclic voltammograms in this study (Figure 1, hydroquinone−quinone). Carbon corrosion is illustrated in Figure 7 by smaller carbon particles. Once a platinum particle loses contact with carbon or the rest of the electronic conductive elements, even still connected with ionomer, there will be no electrode reaction. Consequently, electrochemical reactions cease on the platinum particle and the dissolution stops. A similar scheme also applies to ionomer degradation. This might explain why at higher temperature, there is lower degree of Pt dissolution for both CIEs and HMEAs, on account of higher rate of carbon corrosion or ionomer degradation.

The degradation of Nafion has been reported by others in connection with various applications.[49−51] Ionomer degradation influences the protonic conductivity of the electrode. This is even more critical for HMEA and FMEA, because the ionomer is the only proton conducting phase. This was reflected by the higher CECSA value of CIE20s than HMEA20s (Table 4). Ionomer degradation is illustrated in Figure 7 by segments of fluorocarbon backbone and the loss of side chain and sulfonic acid group after the potential cycling. A considerable expansion of the catalyst layer after potential cycling was also observed using microscopy for both CIE and HMEA samples (section 3.4). This is probably due to a reorientation of the ionomers in aqueous media under the influence of potential field to reach a more thermodynamically stable structure. Such freedom is restricted in FMEA because of the liquid free environment and pressure from both graphite plates.

Preliminary study with X-ray photoelectron spectroscopy has confirmed the degradation of ionomer (and carbon), which might be due to the residual oxygen induced radical formation and polymer dissolution.[52] The result of this study will be published elsewhere.

4.6. Platinum Particle Aggregation. As aforementioned, the crystalline contribution of Nafion ionomer diffraction interferes with platinum (111) plane in the XRD study. The

particle size calculated based on peak widening may not be accurate. Besides, the degradation of the ionomer is hard to be quantified. The relative potential shift of platinum oxide based on electrochemistry might be more precise in predicting catalyst size change (Table 1) than XRD, especially as it represents exclusively electrochemically active platinum; inactive catalysts due to carbon corrosion or ionomer degradation will not be visible in cyclic voltammetry, though they still exist as electrode components.

As indicated by Table 1, ionomer containing samples showed relatively smaller potential shift (or a lower degree of Pt particle aggregation). This is probably due to the interactions between catalyst, carbon support and ionomer. The intimate contact between ionomer and catalyst and supporting carbon formed by physical mixing can prevent platinum particle from coalescence. Furthermore, the lamination by hot pressing was even more effective in preventing platinum particle growth. The consequent electrode structure plays a vital role in catalyst stability and degradation behavior. Higher temperature in general promotes particle movement. This led to a bigger shift of the peak position (more Pt aggregation) in all the cases. The degradation of ionomer may be more severe under single cell operation condition due to radical attack.[53] This can explain the bigger degree of Pt aggregation for FMEAs than HMEAs.

4.7. Laminated Electrode Structure and Catalyst Utilization. On the basis of the evidence from electrochemistry, XRD and microscopy studies, an intense interaction between the ionomers or ionomer-catalyst happened during the lamination procedure. At the same time, this leads to a much compact structure (section 3.4), as illustrated in Figure 7c, d. The laminated ionomer phase turns out to be more stable toward the treatment; the compact electrode structure renders the electrode a sound electronic and protonic contact. Therefore, platinum catalyst shows an improved durability due to the more robust electrode structure as reflected by the higher CECSA values of HME70s than CIE70s.

An interesting trend shown in Table 4, the utilization of CIE20 and HMEA20 was bigger than 100%. In addition, HMEA70, FMEA20 and FMEA70 showed utilization higher than their individual pristine states. These indicate that the surface roughness (or porosity) of the platinum particle increases due to the potential cycling. Though the overall platinum particle size increase in all the cases as reflected by XRD (3.2) and CV (3.1), the total Pt surface area does not necessarily decrease, as illustrated in Figure 7e.

4.8. In Situ Measurement. FMEAs exhibited less stability than HMEAs, as shown in Figure 2 and Table 4 of faster reduction of ECSA and CECSA, Table 1 of bigger platinum oxide reduction peak position shift, and Table 2 of slightly larger relative particle size.

The different performance of FMEA comparing to HMEA is due to a degradation of the complete electrode structure in FMEA including interphase morphology, membrane electrolyte and reference electrode (also used as anode). The observed platinum band (Figure 6a, b) in the membrane is well-known for accelerating membrane degradation, especially pinhole formation.[54] Once pinhole formation occurs in the membrane, it will further enhance gases crossover and performance degradation. Such degradation is specific for FMEA due to its more intricate reaction environment in a single cell, and not observed for HMEA. Moreover, indicated by XRD, platinum particle growth also happens on the anode of FMEA, despite reducing environment (H_2 purging) was applied during the entire experiment.

As a result, the faster Pt area loss for FMEA compared to HMEA is due to a combination of carbon corrosion, ionomer degradation in the catalyst layer and membrane degradation, which are possibly accelerated by the residual radicals[52] generated by hydrogen and/or oxygen crossover during fuel cell operation, especially at elevated temperatures.

5. CONCLUSION

The idea of this work is to compare the differences in catalyst performance and durability carried out through various ex situ and in situ studies. An innovative ex situ experimental electrode design mimicking in situ electrode structure is proposed, where protons are conducted solely through a solid state ionomer phase. The electrochemical stability of the platinum catalyst under a simulated stat/stop cycle was found to be improved by Nafion ionomer homogeneously dispersed in the electrode. This is due to catalyst, support, and the ionomer interaction: ionomer can effectively keep the Pt catalyst from aggregation and detachment from the support; moreover it also alleviates carbon corrosion. Laminated electrode samples displayed even higher durability probably because of the strong binding between ionomer and catalyst, and compact electrode structure. It was found that the roughness of the nanosized platinum catalysts was increased after potential cycling.

The characterization of HMEA can provide valuable information, which is more relevant for fuel cell structure, due to the use of a true half-cell and a stable reference electrode. Furthermore, it opens more possibilities, such as Pt migration studies. It is highly recommended that catalyst evaluation should take the ionomer phase and the electrode structure into account for their influence on the electrode development.

■ ASSOCIATED CONTENT

Supporting Information

S1 TEM image of the catalyst S2 HMEA cell design S3 cyclicvoltametry on electrodes of different structures at 20 and 70 °C, S4 SEM-EDXS cross section on electrodes of different structures. This material is available free of charge via the Internet at http://pubs.acs.org/.

■ AUTHOR INFORMATION

Corresponding Author

*E-mail: mashu@kbm.sdu.dk. Tel: 45 6550 9186.

Notes

The authors declare no competing financial interest.

■ ACKNOWLEDGMENTS

The authors give thanks for the financial support from the Danish PSO project DuraPEM III 2013-1-12064 and the 4M center. IRD Fuel Cells A/S is appreciated for providing electrodes. Lars Duelund is acknowledged for providing AAS measurement facility.

■ REFERENCES

(1) Wang, Y.; Chen, K. S.; Mishler, J.; Cho, S. C.; Adroher, X. C. A Review of Polymer Electrolyte Membrane Fuel Cells: Technology, applications, and needs on fundamental research. *Appl. Energy* **2011**, *88*, 981−1007.

(2) Shao, Y. Y.; Yin, G. P.; Gao, Y. Z. Understanding and Approaches for the Durability Issues of Pt-Based Catalysts for PEM Fuel Cell. *J. Power Sources* **2007**, *171* (2), 558−566.
(3) Tang, Z.; Poh, C. K.; Lee, K. K.; Tian, Z.; Chua, D. H. C.; Lin, J. Enhanced Catalytic Properties from Platinum Nanodots Covered Carbon Nanotubes for Proton-Exchange Membrane Fuel Cells. *J. Power Sources* **2010**, *195*, 155−159.
(4) Bessel, C. A.; Laubernds, K.; Rodríguez, N. M.; Baker, R. T. K. Graphite Nanofibers as an Electrode for Fuel Cell Applications. *J. Phys. Chem. B* **2011**, *105*, 1115−1118.
(5) Muthuswamy, N.; de la Fuente, J. L.G.; Ochal, P.; Giri, R.; Raaen, S.; Sunde, S.; et al. Towards a Highly-Efficient Fuel-Cell Catalyst: Optimization of Pt Particle Size, Supports and Surface-Oxygen Group Concentration. *Phys. Chem. Chem. Phys.* **2013**, *15*, 3803−3813.
(6) Andersen, S. M.; Borghei, M.; Lund, P.; Elina, Y. R.; Pasanen, A.; Kauppinen, E.; et al. Durability of Carbon Nanofiber (CNF) & Carbon Nanotube (CNT) as Catalyst Support for Proton Exchange Membrane Fuel Cells. *Solid State Ionics* **2013**, *231*, 94−101.
(7) Dhiman, R.; Johnson, E.; Skou, E.; Morgen, P.; Andersen, S. M. SiC Nanocrystals as Pt Catalyst Supports for Fuel Cell Applications. *J. Mater. Chem. A* **2013**, *1*, 6030−6036.
(8) Dhiman, R.; Stamatin, S. N.; Andersen, S. M.; Morgen, P.; Skou, E. Oxygen Reduction and Methanol Oxidation Behaviour of SiC Based Pt Nanocatalysts for Proton Exchange Membrane Fuel Cells. *J. Mater. Chem. A* **2013**, *1*, 15509−15516.
(9) Perchthaler, M.; Ossiander, T.; Juhart, V.; Mitzel, J.; Heinzl, C.; Scheu, C.; Hacker, V. Tungsten Materials as Durable Catalyst Supports for Fuel Cell Electrodes. *J. Power Sources* **2013**, *243*, 472−480.
(10) Takenaka, S.; Kishida, M. Functionalization of Carbon Nanotube-Supported Precious Metal Catalysts by Coverage with Metal Oxide Layers. *Catal. Surv. Asia* **2013**, *17* (2), 71−84.
(11) Xu, F.; Wang, M. X.; Sun, L. L.; Liu, Q.; Sun, H. F.; Stach, E. A.; Xie, J. Enhanced Pt/C Catalyst Stability using P-benzensulfonic Acid Functionalized Carbon Blacks as Catalyst Supports. *Electrochim. Acta* **2013**, *94*, 172−181.
(12) He, D. P.; Mu, S. C.; Pan, M. Perfluorosulfonic Acid-functionalized Pt/carbon Nanotube Catalysts with Enhanced Stability and Performance for Use in Proton Exchange Membrane Fuel Cells. *Carbon* **2011**, *49*, 82−88.
(13) Cheng, N. C.; Mu, S. C.; Chen, X. J.; Lv, H. F.; Pan, M.; Edwards, P. P. Enhanced Life of Proton Exchange Membrane Fuel Cell Catalysts using Perfluorosulfonic Acid Stabilized Carbon Support. *Electrochim. Acta* **2011**, *56*, 2154−2159.
(14) Curnick, O. J.; Mendes, P. M.; Pollet, B. J. Enhanced Durability of a Pt/C Electrocatalyst Derived from Nafion-stabilised Colloidal Platinum Nanoparticles. *Electrochem. Commun.* **2010**, *12*, 1017−1020.
(15) Balberg, I. Tunneling and Nonuniversal Conductivity in Composite-Materials. *Phys. Rev. Lett.* **1987**, *59*, 1305−1308.
(16) Rubatat, L.; Gebel, G.; Diat, O. Fibrillar structure of Nafion: Matching Fourier and Real Space Studies of Corresponding Films and Solutions. *Macromolecules* **2004**, *37*, 7772−7783.
(17) Andersen, S. M.; Grahl-Madsen, L.; Skou, E. Studies on PEM Fuel Cell Noble Metal Catalyst Dissolution. *Solid State Ionics* **2011**, *192*, 602−606.
(18) Choi, S.; Jung, D.; Yoon, S.; Park, S.; Oh, E.; Junbom, K. Optimum Content of Nafion Ionomer for the Fabrication of MEAs in PEMFCs with Spray-Coated Pt/CNT Electrodes. *Met. Mater. Int.* **2011**, *17*, 811−816.
(19) Li, W.; Waje, M.; Chen, Z.; Larsen, P.; Yan, Y. Platinum Nanopaticles Supported on Stacked-Cup Carbon Nanofibers as Electrocatalysts for Proton Exchange Membrane Fuel Cell. *Carbon* **2010**, *48*, 995−1003.
(20) Tucker, M. C.; Odgaard, M.; Lund, P. B.; Yde-Andersen, S.; Thomas, J. O. The Pore Structure of Direct Methanol Fuel Cell Electrodes. *J. Electrochem. Soc.* **2005**, *152* (9), A1844−A1850.
(21) Bass, M.; Berman, A.; Singh, A.; Konovalov, O.; Freger, V. Surface-Induced Micelle Orientation in Nafion Films. *Macromolecules* **2011**, *44*, 2893−2899.
(22) Hiraoka, F.; Matsuzawa, K.; Mitsushima, S. Degradation of Pt/C Under Various Potential Cycling Patterns. *Electrocatalysis* **2013**, *4*, 10−16.
(23) Fultz, D. W.; Chuang, P. Y. A. The Property and Performance Differences Between Catalyst, Coated Membrane and Catalyst Coated Diffusion Media. *J. Fuel Cell Sci. Technol.* **2011**, *8*, 041010−1.
(24) Okur, O.; Karada, C. L.; San, F. J. B.; Okumus, E.; Behmenyar, G. Optimization of Parameters for Hot-Pressing Manufacture of Membrane Electrode Assembly for PEM (Polymer Electrolyte Membrane Fuel Cells) Fuel Cell. *Energy* **2013**, *57*, 574−580.
(25) Jia, S.; Liu, H. Cold Pre-Compression of Membrane Electrode Assembly for PEM Fuel Cells. *Int. J. Hydrogen Energy* **2012**, *37*, 1367−13680.
(26) He, Q. P.; Joy, D. C.; Keffer, D. J. Nanoparticle Adhesion in Proton Exchange Membrane Fuel Cell Electrodes. *J. Power Sources* **2013**, *241*, 634−646.
(27) Ma, S.; Chen, Q.; Jøgensen, F.; Stein, P.; Skou, E. ^{19}F NMR Studies of Nafion Ionomer Adsorption on PEMFC Catalysts and Supporting Carbons. *Solid State Ionics* **2007**, *178*, 1568−1575.
(28) Andersen, S. M.; Borghei, M.; Dhiman, R.; Jiang, H.; Ruiz, V.; Kauppinen, E.; Skou, E. Interaction of Multi-Walled Carbon Nanotubes with Perfluorinated Sulfonic Acid Ionomers and Surface Treatment Studies. *Carbon* **2014**, *71*, 218−228.
(29) Andersen, S. M.; Borghei, M.; Dhiman, R.; Ruiz, V.; Kauppinen, E.; Skou, E. Adsorption Behavior of Perfluorinated Sulfonic Acid Ionomer on Highly Graphitized Carbon Nanofibers and Their Thermal Stabilities. *J. Phys. Chem. C* **2014**, *118*, 10814−10823.
(30) Durst, J.; Lamibrac, A.; Charlot, F.; Dillet, J.; Castanheira, L. F.; Maranzana, G.; Dubau, L.; Maillard, F.; Chatenet, M.; Lottin, O. Degradation Heterogeneities Induced by Repetitive Start/Stop Events in Proton Exchange Membrane Fuel Cell: Inlet vs. Outlet and Channel vs. Land. *Appl. Catal., B* **2013**, *138−139*, 416−426.
(31) Tintula, K. K.; Jalajakshi, A.; Sahu, A. K.; Pitchumani, S.; Sridhar, P.; Shukla, A. K. Durability of Pt/C and Pt/MC-PEDOT Catalysts under Simulated Start-Stop Cycles in Polymer Electrolyte Fuel Cells. *Fuel Cells* **2012**, *13*, 158−166.
(32) http://www.jmj.co.jp/fuel/img/hispec_catalysts_internal_oct_06_1.pdf.
(33) Eliezer, G. *Electrode Kinetics for Chemists, Chemical Engineers, and Materials Scientists*; VCH: Weinheim, Germany, 1993.
(34) Loo, B. H.; Furtak, T. E. Intrinsic Heterogeneity in the Multiple States of Adsorbed Hydrogen on Polycrystalline Platinum. *Electrochim. Acta* **1980**, *25*, 505−508.
(35) Kinoshita, K.; Stonehart, P. Role of Platinum Morphology on Hydrogen Adsorption Isotherms − IV. *Electrochim. Acta* **1975**, *20*, 101−107.
(36) Frelink, T.; Visscher, W.; van Veen, J. A. R. The Third Anodic Hydrogen Peak on Platinum; Subsurface H2 Adsorption. *Electrochim. Acta* **1995**, *40*, 545−549.
(37) Gasteiger, H. A.; Kocha, S. S.; Sompalli, B.; Wagner, F. T. Activity Benchmarks and Requirements for Pt, Pt-alloy, and Non-Pt Oxygen Reduction Catalysts for PEMFCs. *Appl. Catal., B* **2005**, *56*, 9−35.
(38) Moore, R. B., III; Martin, C. R. Chemical and Morphological Properties of Solution-Cast Perfluorosulfonate Ionomers. *Macromolecules* **1988**, *21*, 1334−1339.
(39) Bi, W.; Gray, G. E.; Fuller, T. F. PEM fuel cell Pt/C Dissolution and Deposition in Nafion Electrolyte. *Electrochem. Solid-State Lett.* **2007**, *10* (5), B101−B104.
(40) Berejnov, V.; Martin, Z.; West, M.; Kundu, S.; Bessarabov, D.; Stumper, J.; Susac, D.; Hitchcock, A. P. Probing Platinum Degradation in Polymer Electrolyte Membrane Fuel Cells by Synchrotron X-ray Microscopy. *Phys. Chem. Chem. Phys.* **2012**, *14*, 4835−4843.
(41) Uchida, M.; Park, Y. C.; Kakinuma, K.; Yano, H.; Tryk, D. A.; Kamino, T.; Uchidab, H.; Watanabe, M. Effect of the State of Distribution of Supported Pt Nanoparticles on Effective Pt Utilization in Polymer Electrolyte Fuel Cells. *Phys. Chem. Chem. Phys.* **2013**, *15*, 11236−11247.

(42) Malek, K.; Mashio, T.; Eikerling, M. Microstructure of Catalyst Layers in PEM Fuel Cells Redefined: A Computational Approach. *Electrocatalysis* **2011**, *2*, 141−157.
(43) Joo, S. H.; Pak, C.; You, D. J.; Lee, S. A.; Lee, H. I.; Kim, J. M.; Chang, H.; Seung, D. Ordered Mesoporous Carbons (OMC) as Supports of Electrocatalysts for Direct Methanol Fuel Cells (DMFC): Effect of Carbon Precursors of OMC on DMFC Performances. *Electrochim. Acta* **2006**, *52*, 1618−1626.
(44) Yuan, T.; Zhang, H.; Zou, Z.; Khatun, S.; Akins, D.; Adam, Y.; Suarez, S. A Study of the Effect of Heat-Treatment on the Morphology of Nafion Ionomer Dispersion for Use in the Passive Direct Methanol Fuel Cell (DMFC). *Membranes* **2012**, *2*, 841−854.
(45) Pak, C.; Chang, H.; Kim, J. Method of Manufacturing Hierarchical Mesopores Carbon and Carbon Obtained Hereby, *US Pat. Appl. Publ.*, US 2012/0196745 A1.
(46) Paul, D. K.; Fraser, A.; Pearce, J.; Karan, K. Understanding the Ionomer Structure and the Proton Conduction Mechanism in PEFC Catalyst Layer: Adsorbed Nafion on Model Substrate. *ECS Trans.* **2011**, *41* (1), 1393−1406.
(47) Li, X.; Feng, F.; Zhang, K.; Ye, S. U.; Kwok, D. Y.; Birss, V. Wettability of Nafion and Nafion/Vulcan Carbon Composite Films. *Langmuir* **2012**, *28*, 6698−6705.
(48) Xu, F.; Wang, M. X.; Liu, Q.; Sun, H:F.; Simonson, S.; Ogbeifun, N.; Stach, E. A.; Xie, J. Investigation of the Carbon Corrosion Process for Polymer Electrolyte Fuel Cells Using a Rotating Disk Electrode Technique. *J. Electrochem. Soc.* **2010**, *157* (8), B1138−B1145.
(49) Hsieh, Y. C.; Chen, J. Y.; Wu, P. W. Electrochemical Degradation of Nafion Ionomer to Functionalize Carbon Support for Methanol Electro-Oxidation. *J. Power Sources* **2011**, *196*, 8225−8233.
(50) Chen, C.; Fuller, T. F. The Effect of Humidity on the Degradation of Nafion Membrane. *Polym. Degrad. Stab.* **2009**, *94*, 1436−1447.
(51) Lee, H. J.; Cho, M. K.; Jo, Y. Y.; Lee, K. S.; Kim, H. J.; Cho, E.; et al. Application of TGA Techniques to Analyze the Compositional and Structural Degradation of PEMFC MEAs. *Polym. Degrad. Stab.* **2012**, *97*, 1010−1016.
(52) Jao, T. C.; Jung, G. B.; Kuo, S. C.; Tzeng, W. J.; Su, A. Degradation mechanism study of PTFE/Nafion membrane in MEA utilizing an accelerated degradation technique. *Int. J. Hydrogen Energy* **2012**, *37*, 13623−13630.
(53) Ghassemzadeh, L.; Marrony, M.; Barrera, R.; Kreuer, K. D.; Maier, J.; Müller, K. Chemical Degradation of Proton Conducting Perfluorosulfonic Acid Ionomer Membranes Studied by Solid-State Nuclear Magnetic Resonance Spectroscopy. *J. Power Sources* **2009**, *186*, 334−338.
(54) Ohma, A.; Yamamoto, S.; Shinohara, K. Membrane Degradation Mechanism during Open-Circuit Voltage Hold Test. *J. Power Sources* **2008**, *182*, 39−47.